AIAA SciTech Forum
8-12 January 2024, Orlando, FL
AIAA SCITECH 2024 Forum

10.2514/6.2024-1957

Inferring Electron Heat Flux in a High-Power Hall Thruster with Incoherent Thomson Scattering

Parker J. Roberts* and Benjamin A. Jorns †
University of Michigan, Ann Arbor, Michigan, 48109

The electron heat flux is experimentally determined with laser diagnostics in the plume of a 9-kW-class, magnetically shielded Hall thruster. An incoherent Thomson scattering system is used to determine the electron density and temperature along the azimuthal direction on channel centerline. Additionally, laser-induced fluorescence is employed to measure the axial velocities of singly-charged ions. These measurements are combined with a simplified electron energy transport equation in the axial direction, across the confining magnetic field. From this model, statistical techniques are implemented to provide profiles of the anomalous electron heat flux as a function of axial position. It is found that electron temperatures measured with this technique exceed predictions made with state-of-the-art fluid codes based on near-field probe measurements by a factor of 2-2.5. In addition, the electron heat flux inferred directly from these measurements does not agree with collisional formulations for energy transport, contrary to existing fluid models of electron energy flux in crossed-field plasmas. The values of this experimental heat flux are primarily driven by large plasma convection across field lines from this region of relatively hot electrons. This discrepancy with collisional formulations strongly suggests that the anomalous electron thermal conductivity may not be accurately described by the momentum-transfer collision rate.

I. Introduction

Hall thrusters are widely-flown space propulsion devices which produce thrust by accelerating a crossed-field plasma [1, 2]. These devices work by using a radial magnetic field to confine electrons in an annular plasma channel. These trapped electrons then mediate the transfer of electrostatic energy from applied fields to the directed kinetic energy of ions. Because of this key role played by the electrons, the loss of electron confinement due to their diffusion across this magnetic field represents both a direct efficiency loss as well as a sensitive determinant of plasma properties [1, 3, 4]. For this reason, a detailed accounting of cross-field momentum and energy transport in the Hall thruster plume is essential for understanding performance trends as well as modeling these devices self-consistently.

Classically, the transit of electron energy and momentum across a confining magnetic field occurs due to collisions with heavy particles [5]. In practice, however, the rate of electron flux is orders of magnitude larger than can be explained by classical collisions in low-temperature, crossed-field plasmas such as Hall thrusters [2, 6]. Despite extensive research into first-principles explanations of this so-called "non-classical" diffusion, such as interactions with plasma turbulence or the solid walls [6–9], the behavior remains poorly understood. Rather than predict this high cross-field transport from first principles, then, it is instead a common practice to account for the unknown forces and energy fluxes using macroscopic transport coefficients in a fluid model for the electron motion [10–13]. These transport coefficients are then tuned until model results agree with experimental measurements [4, 12, 14]. While this model inversion approach has proven effective for understanding much of the local plasma behavior in Hall thrusters [15–17], there are limitations in the assumptions widely used for such models that remain unchecked by direct and non-invasive experimental tests.

One such limitation is a form for the cross-field thermal conductivity which assumes the same effective electron collision frequency as is required to account for momentum transport. For example, some models infer an effective collision frequency as a coefficient in a drag-force-like term in the momentum equation [4, 11, 12], which is calibrated from measurements of ion velocities in the thruster plume [10, 16]. The tendency of electrons to conduct internal energy across field lines is then computed based on a classical, collisional formulation, but with this effective collision frequency substituted in favor of the classical value. However, there exist few non-invasive measurements to validate the terms in the electron energy equation. Some probe-based electron temperature measurements exist [18–20], but these have significant uncertainties due to the perturbative nature of injected plasma probes [20, 21]. Furthermore, models

*Doctoral Candidate, Department of Aerospace Engineering, AIAA Student Member.
†Associate Professor, Department of Aerospace Engineering, AIAA Associate Fellow.

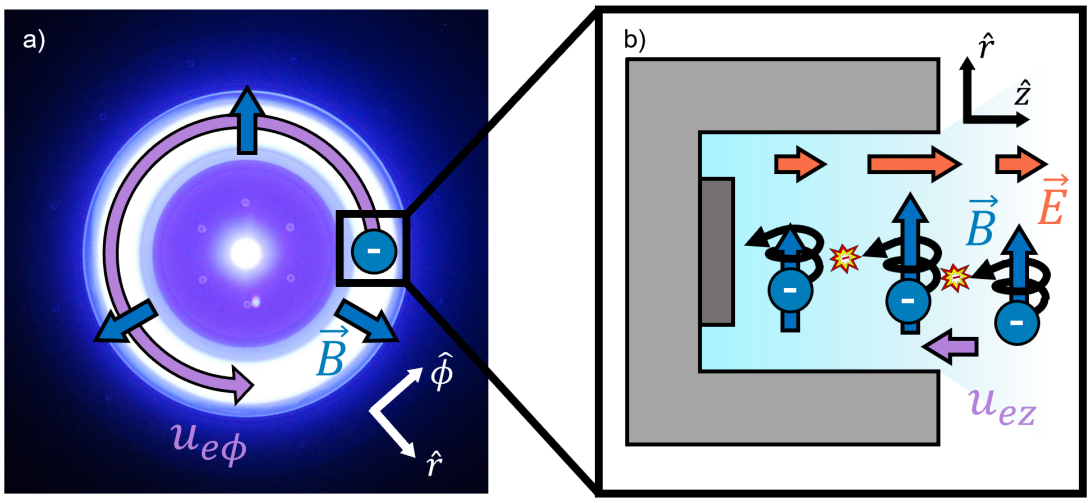

Fig. 1 a) Photograph of the H9 Hall thruster operating on krypton at 300 V, 15 A, with radial magnetic field and azimuthal electron drift overlaid. b) Illustration of electron behavior in the Hall thruster channel, notionally showing the collision-driven migration of electrons in the axial, cross-field direction.

informed by these probing studies exhibit significant discrepancies with recent non-invasive experimental measurements of Hall thruster electron temperatures [7, 13, 15, 22, 23]. There is thus a pressing need to experimentally investigate the local cross-field heat transport characteristics of the electron population within the acceleration region of a Hall thruster.

In this work, we address this need with a combined laser scattering approach to non-invasively measure the axial electron heat flux on channel centerline of a laboratory Hall thruster. To this end, in Sec. II we review the operation of Hall thrusters and develop a formulation for the heat flux in terms of electron heating and loss mechanisms. Following this, Sec. III describes a suite of laser scattering diagnostics to measure the unknown plasma quantities in this energy equation and thus infer the local variation of the electron heat flux. Section IV then presents the results of these experiments, while in Sec. V we discuss our heat flux measurements in the context of common assumptions used to model crossed-field plasmas. Section VI then summarizes the implications of these results.

II. Theory

In this section, we first summarize the physics governing Hall thruster operation, including an Ohm's law description of plasma diffusion. After this, we invoke the electron energy conservation equation as a tool for inferring the local heat flux in the plasma. Finally, we quote classical results to describe this heat flux for comparison with our measurements.

A. Hall Thruster Operation and Electron Momentum Transport

Figure 1 illustrates the basic features of Hall thruster operation. As discussed in the preceding, these devices work on the principle of accelerating ions with an axial electric field, $\vec{E} = E_z\hat{z}$, which is maintained within a quasineutral plasma. This state is accomplished by employing a radial magnetic field, $\vec{B} = B_r\hat{r}$, across an annular plasma channel. The strength of B_r is chosen to be of sufficient strength to magnetize electrons, but not ions. The resulting "crossed-field" plasma configuration impedes the axial motion of electrons; this effectively forces a high plasma resistivity in the region of large magnetic field, which in turn localizes the potential difference between the anode and cathode and allows a large electric field to be reached. Additionally, this high plasma resistivity leads to Ohmic electron heating, allowing the hot, trapped electrons to ionize propellant in a region just upstream of the peak magnetic field. A byproduct of this configuration is a strong electron drift, $u_{e\phi}$, in the $E \times B$ (azimuthal) direction (c.f. Fig. 1a).

As shown in Fig. 1b, the diffusion of electrons across the magnetic field in the axial direction, at speed u_{ez}, is

classically attributed to collisions with ions and neutrals. These collisions randomize the direction of the electron velocity, promoting random-walk-like motion in the direction of the electric force [5]. A simple but powerful description of this process may be obtained with a generalized Ohm's law,

$$u_{e\phi} = \frac{1}{1+\Omega^{-2}}\left(\frac{E_z}{B_r} + \frac{d(n_e k_B T_e)/dz}{e n_e B_r}\right), \tag{1}$$

$$u_{ez} = \frac{\Omega^{-1}}{1+\Omega^{-2}}\left(\frac{E_z}{B_r} + \frac{d(n_e k_B T_e)/dz}{e n_e B_r}\right), \tag{2}$$

where e is the fundamental charge, n_e is the electron density, T_e is the electron temperature, and Ω is the Hall parameter, which represents the ratio of the cyclotron frequency for electrons with mass m_e, $\omega_{ce} = eB_r/m_e$, to the electron collision frequency, ν_e. This expression represents the conservation of momentum for electrons, neglecting inertia. For the strongly magnetized case ($\Omega^{-1} \ll 1$), the azimuthal $E \times B$ electron drift is moderated by the diamagnetic effect, resulting from a negative axial gradient in the plasma pressure $p_e = n_e k_B T_e$. Meanwhile, the effect of increasing the effective collision rate $\propto \Omega^{-1}$ is to redirect this drift energy partially into the axial direction. We therefore see from Eq. 2 that the inverse Hall parameter, Ω^{-1}, is a normalized coefficient which regulates the rate of electron momentum transport across the magnetic field due to collisions. The inverse Hall parameter is commonly treated as a tunable, effective transport coefficient in models, which accounts for both classical and non-classical effects [11, 12, 15]. In Ref. [23], we used this formulation to infer the effective value of the inverse Hall parameter in a Hall thruster discharge using non-intrusive plasma measurements. However, this previous investigation did not address the unknown physics related to transport of electron energy, which we discuss in the following.

B. Electron Energy Equation

To investigate the ability of electrons to transport energy in the plasma, we consider the internal energy conservation equation for the electron species [1],

$$\frac{3}{2}\frac{\partial p_e}{\partial t} + \nabla \cdot \left(\frac{5}{2} p_e \vec{u}_e\right) = \vec{E} \cdot \vec{J}_e - \dot{n}\varepsilon_{iz} - \nabla \cdot \vec{\theta}_e. \tag{3}$$

This expression describes the evolution in space and time of the electron pressure. The terms on the left hand side, which account for unsteady pressure variation and the convection of thermal energy at bulk electron velocity $\vec{u}_e$, are balanced by the Ohmic heating effect $\vec{E} \cdot \vec{J}_e$, where $\vec{J}_e$ is the electron current density. The right-hand-side of Eq. 3 also includes additional electron heat losses, such as the loss of the ionization energy ε_{iz} for each ionization collision, occuring at frequency $\dot{n}$ per unit volume, along with the tendency of the electron fluid to conduct heat internally, parameterized by the heat flux density, $\vec{\theta}_e$. Classically, $\vec{\theta}_e$ represents heat diffusion which arises from gradient-driven deviations from thermodynamic equilibrium, accounted for by collisional effects. Much like diffusion of electron momentum across field lines, however, the heat flux consistent with experiments suggests effective collision frequencies that greatly exceed the rates predicted by classical collisions alone [11]. Therefore, the parameter θ_{ez} is commonly used to represent an effective energy transport term which accounts for unknown, kinetic effects within the fluid framework, such as interaction between the electrons and plasma turbulence, in addition to classical collisions.

In this work, we restrict our attention to the variation of local plasma properties along channel centerline, and make the steady-state assumption. Due to the difficulty of measuring the small, axial electron migration velocity u_{ez}, we represent the axial electron current density subtractively as $\vec{J}_e = \vec{J}_{tot} - \vec{J}_i$, where $\vec{J}_{tot}$ is the total current density and $\vec{J}_i = e n_e u_{iz} \hat{z}$ is the ion current density. In addition to assuming that the magnetic field is purely radial and the electric field is purely axial along this axis, we assume by device symmetry that gradients in the radial and azimuthal direction are negligible at the center of the channel. Considering that the ion production rate, $\dot{n}$, is determined by the 1D, steady-state ion continuity equation, $\dot{n} = d(n_i u_{iz})/dz$, we can rewrite Eq. 3 as

$$\frac{d\theta_{ez}}{dz} = E_z\left(J_{z,tot} - e n_e u_{iz}\right) - \frac{d}{dz}\left(\frac{5}{2} n_e k_B T_e \left[u_{iz} - \frac{J_{z,tot}}{ne}\right] - \varepsilon_{iz} n_e u_{iz}\right) \tag{4}$$

This expression shows that subject to the assumptions above, the change in the electron heat flux with axial location can be directly determined from measurements of the electron pressure, density, and axial velocity, in addition to the ion velocity and plasma potential. Next, we explore classical assumptions for collisional heat flux scaling which are commonly employed in models.

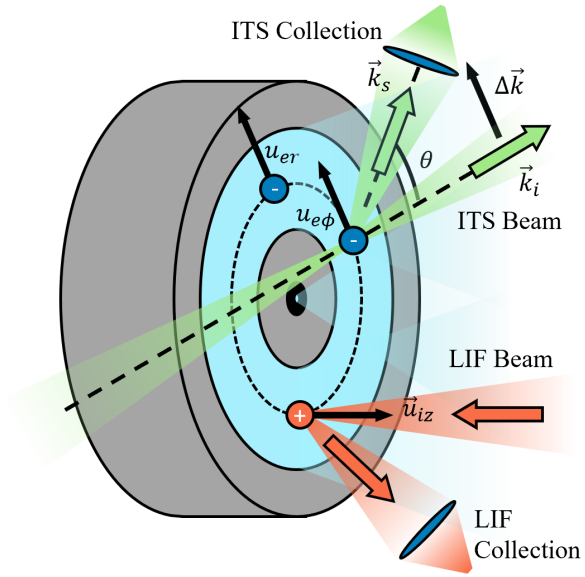

Fig. 2 Schematic of the laser injection geometry for the ITS and LIF investigations.

C. Classical Heat Conduction

The classical description of the heat flux density typically makes use of a thermal conductivity coefficient, κ_e, in a Fourier law:

$$\vec{\theta} = -\kappa_e \nabla T_e. \tag{5}$$

Following Braginskii [24, 25], for a plasma with strong ionization and magnetization, the value of this coefficient for transport perpendicular to field lines is given by

$$\kappa_\perp = 4.7 \frac{n_e k_B^2 T_e \nu_{ei}}{m_e \omega_{ce}^2}, \tag{6}$$

where ν_{ei} represents the frequency of electron collisions which transfer momentum to singly-charged ions. The value of ν_{ei} can in turn be determined as

$$\nu_{ei} = \frac{n_e e^4 \ln\Lambda}{6\epsilon_0^2 \sqrt{2m_e}(\pi k_B T_e)^{3/2}}, \tag{7}$$

where ϵ_0 is the free-space permittivity and $\ln\Lambda$ is the Coulomb logarithm [25]. Equations 6-7 accounts for the reduced transport of energy due to the magnetic field's impeding effect on cross-field electron migration. Analogously to Eq. 2, increasing the value of the collision rate, ν_{ei}, has the effect of enhancing this cross-field energy transport. Like the inverse Hall parameter, then, it is a common approach to treat $\kappa_{e\perp}$ as an effective transport parameter which can be tuned to account for non-classical, enhanced energy transport in fluid models. This is typically done by substituting the effective value of ν_e inferred from Eq. 2 in for the classical collision rate in Eq. 6 [4, 11, 12]. In the following, we describe a series of laser scattering experiments in order to measure these plasma properties to determine the cross-field electron heat flux, thereby evaluating the validity of this approximation.

III. Experiment

In this section, we describe the apparatus for a combined laser scattering experiment, leveraging both laser-induced fluorescence and incoherent Thomson scattering, in order to measure the local plasma properties required to infer the electron heat flux from Eq. 4.

A. Facility and Thruster

We performed this investigation on the H9 Hall thruster, a 9-kW class, magnetically shielded Hall thruster developed in collaboration between the University of Michigan, the Air Force Research Laboratory, and the Jet Propulsion Laboratory [26]. We operated the H9 in the Alec D. Gallimore Large Vacuum Test Facility with krypton propellant, at a discharge voltage of 300 V and a discharge current of 15 A [27]. During thruster firing, the background pressure in the facility was maintained at 5 µTorr-krypton, as measured by a Stabil ion gauge in the exit plane of the thruster, per best practices recommendations [28]. We operated the thruster with the hollow cathode potential electrically tied to the thruster body.

B. Laser-Induced Fluorescence Experiment

We first investigated the electrostatic acceleration of ions in the H9 using a laser-induced fluorescence (LIF) diagnostic. This apparatus, which is described in detail in Ref. [16], enables inference of the ion velocity distribution from the Doppler-broadened lineshape of an electronic transition from a metastable state of singly-ionized krypton. We tuned the wavelength of a diode laser in a range around the transition at 728.98 nm (air) to accomplish this. We employed fiber-coupled injection optics within the vacuum facility to focus the beam to a sub-mm spot in the thruster plume. As shown in Fig. 2, this beam entered the plume axially, allowing measurement of the axial ion velocity; the fluorescent light at 473.90 nm which resulted from this stimulated excitation then was collected by a 75-mm-diameter oblique collection optic. The collected light was fiber-coupled to a photomultiplier tube outside of the chamber, where bandpass filtering was applied around the expected fluorescence wavelength. Additionally, we improved signal-to-noise by modulating the laser with a mechanical chopper and employing an analog lock-in amplifier to perform phase-sensitive detection of the LIF signal. Translating the thruster on a 3-axis motion stage allowed for characterization of the evolution of the ion velocity distribution along the axial direction on channel centerline.

C. Incoherent Thomson Scattering Experiment

To measure the electron properties, we used an incoherent Thomson scattering (ITS) diagnostic. Analogously to LIF, this diagnostic scatters laser light from the free electrons in the plasma in order to infer the electron velocity distribution function (EVDF) from the Doppler shift in the resulting spectrum. For this experiment, we injected an Nd:YAG, Q-switched laser with a wavelength of 532 nm into the plasma horizontally, as shown in Fig. 2. We oriented the polarization of the beam in the axial direction of the thruster. Each laser pulse emitted ~ 700 mJ of energy within 10 ns, with a repetition rate of 10 Hz. We focused the laser into the plasma with a Galilean telescope, consisting of a concave and convex lens with high-energy coatings in series. After these optics, the beam passed through a vacuum window and reached the thruster plume by way of a motorized periscope within the chamber. The effective focal length was approximately 6 meters, leading to a spot diameter ~1 mm. A 1-cm-diameter aperture in an aluminum plate, mounted halfway along this focal path, acted as a stray light shield. This shielding reduced the probability of large-angle beamlets, such as those scattered randomly from optic surfaces, surviving at the thruster. A water-cooled beam dump then collected the unscattered remnant of the beam on the far side of the vacuum chamber.

Meanwhile, we collected scattered light at an angle $\theta = 30^\circ$ to the incident wavevector, as shown in Fig. 2. We accomplished this with an in-situ dual-lens, 75-mm-diameter optic placed 200 mm from the laser beam waist, which collected light in a cone with approximate wavevector $\vec{k}_s$. This light was coupled into a 1-mm-diameter optical fiber, which routed the photons to a detection bench outside of the vacuum chamber. The detection apparatus, described in further detail in Ref. [29], collimated the fiber output, followed by a three-stage stray light filtering system based on volume Bragg gratings (VBGs). This stray light filtering strategy was first demonstrated in Ref. [30]. The filtered light then was refocused into an imaging spectrometer through a 500-µm slit, where a 600 g/mm grating diffracted the scattered spectrum onto an EMICCD camera. This detector was operated with an EMI gain of 5000, using a 15-ns exposure window synchronized to the laser pulse. We aligned the optics with the interrogation volume positioned at a clock angle of $\theta/2 = 15^\circ$ from horizontal, which positioned the measurement vector $\Delta\vec{k}$ along the azimuthal direction on channel centerline. At each location, we irradiated the detector with 3000 laser pulses, followed by acquiring 3000 exposures with the laser off. The average of these two acquisition types were then subtracted to eliminate plasma emission lines from the spectrum. Similarly to the LIF system, a three-axis motion stage allowed the thruster to translate relative to the interrogation location for both diagnostics, enabling spatial resolution of 1 mm.

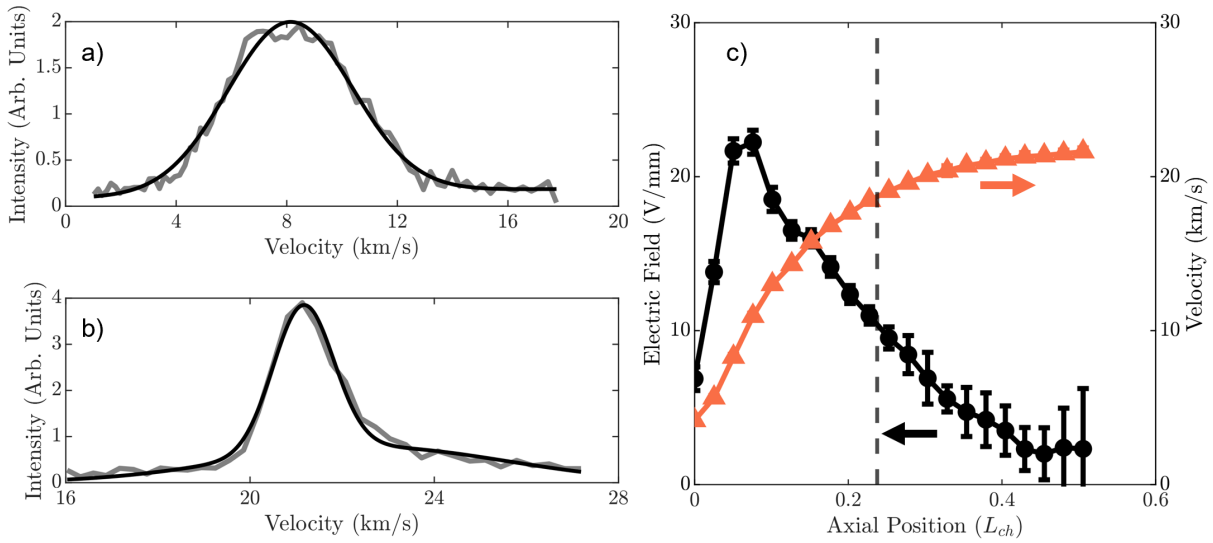

Fig. 3 a) Laser-induced fluorescence measurement of the axial ion velocity distribution, 0.05 channel lengths from the exit plane. b) Laser-induced fluorescence measurement of the axial ion velocity distribution, 0.51 channel lengths from the exit plane. c) Resulting axial ion velocity curve and inferred electric field, with the location of maximum magnetic field shown as a dashed line. Locations are normalized to channel length and referenced to the exit plane. Median estimates are shown, with 95 % credible intervals propagated from the fit uncertainty.

IV. Results

In this section, we first describe our extraction of plasma properties from the LIF and ITS spectra observed along channel centerline in the thruster. Following this, we demonstrate the computation of the terms of the energy equation and subsequent inference of the electron heat flux throughout the Hall thruster plume.

A. Analysis of LIF Spectra

Figures 3a-b) show examples of laser-induced fluorescence traces at two locations in the plasma. The lab-frame laser wavelength is converted to ion velocity v according to the Doppler shift $v(\lambda) = c(\lambda/\lambda_0 - 1)$, where c is the speed of light and λ_0 is the center wavelength of the excitation line. This resulting velocity spectrum is representative of the ion velocity distribution function (IVDF) along the laser axis; non-Doppler broadening effects may be ignored in this region (see Ref. [7]). We fit this LIF data to reduce noise by using a model $f_i(v)$ consisting of the sum of two Maxwellian distributions. From the resulting analytical curves, we computed the mean axial ion velocity by computing the statistical mean,

$$u_{iz} = \frac{\int f_i(v) v dv}{\int f_i(v) dv}. \tag{8}$$

Because the ions are approximately collisionless downstream of the thruster face [4], the axial electric field can be inferred from the evolution of the IVDF. Following the formulation in Ref. [31] based on the first three moments of the Boltzmann equation, we numerically integrated the fitting functions over a fine grid to compute the axial electric field. For derivatives of these moments, we employed smoothing spline fits which could be differentiated analytically.

We produced Monte Carlo statistics for the values of ion velocity and electric field at each location by generating normally distributed ensembles of 10,000 possible fitting parameters for each point, based on the standard error from least-squares minimization. From these empirical distributions, we display median values for ion velocities in addition to this electric field as a function of axial location on channel centerline in Fig. 3. We also display 95% credible intervals for these quantities. We see that the electric field accelerates the ions up to their asymptotic velocity of approximately 25 km/s, with the region of maximum electric field located upstream of the location of maximum magnetic field.

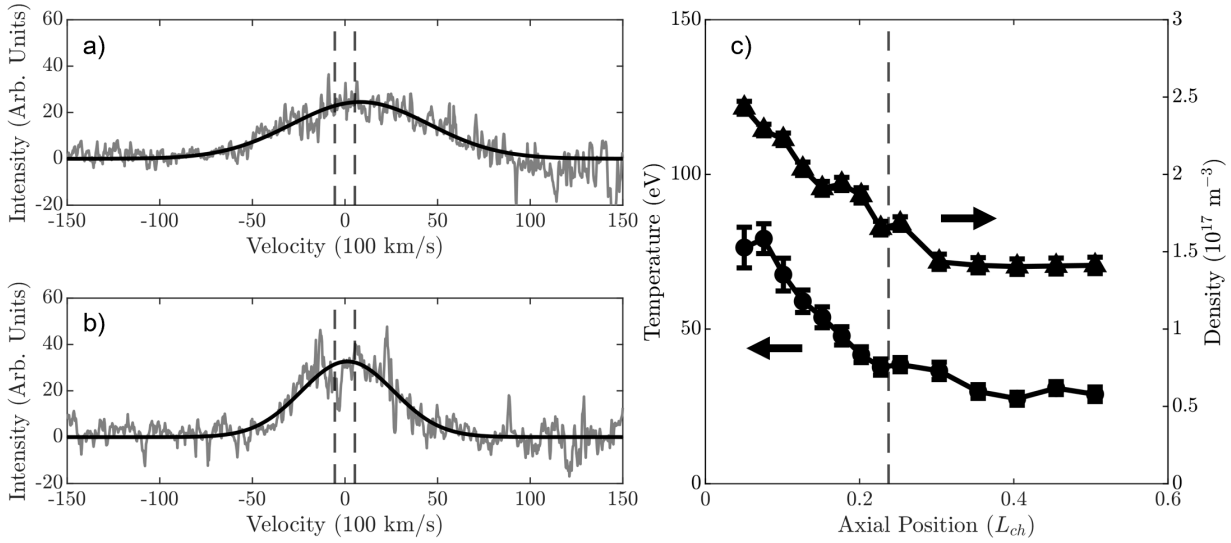

Fig. 4 a) Incoherent Thomson scattering measurement of the axial electron velocity distribution, 0.05 channel lengths from the exit plane. A Maxwellian fit is shown, with points in the notch filter stopband (dashed lines) excluded. b) Incoherent Thomson scattering measurement of the axial electron velocity distribution, 0.51 channel lengths from the exit plane. c) Resulting electron temperature and density profiles, with the location of maximum magnetic field shown as a dashed line. Locations are normalized to channel length and referenced to the exit plane.

B. Analysis of ITS Spectra

Figures 4a-b display Thomson scattering spectra at two locations in the Hall thruster plume. For this experiment, the scattering wavevector magnitude Δk satisfied relationship $\Delta k \lambda_D << 1$, where λ_D is the plasma Debye length. This corresponds to the limit of incoherent Thomson scattering, in which case the scattered spectral intensity is the sum of the power scattered from each electron [32]. We therefore convert the scattered wavelength, λ, into azimuthal electron velocity, v, via the vector Doppler shift relation

$$v(\lambda) = \frac{c(\lambda_0/\lambda - 1)}{2\sin\theta/2}, \tag{9}$$

where $\lambda_0 = 532$ nm is the laser wavelength. We fit these distributions with a model $g(\lambda)$ corresponding to a Maxwellian distribution, convolved with the instrument broadening function $I(\lambda)$:

$$g(\lambda_k) = \sum_{\ell=1}^{N} \frac{H n_e r_e^2}{v_{Te}\sqrt{\pi}} e^{\left(-\frac{(v(\lambda_\ell)-u_e)^2}{v_{Te}^2}\right)} I\left(\lambda_k - \lambda_\ell\right), \tag{10}$$

where N is the number of wavelength bins (camera pixels), r_e is the classical electron radius, $v_{Te} = \sqrt{2k_B T_e/m_e}$ is the electron thermal speed, and H is an intensity calibration factor. We determined $I(\lambda)$ by misaligning the stray light filters and exposing the detector to scattered laser radiation at low gain - this allowed characterization of the broadening effects on the stray light, which is effectively a Dirac distribution relative to the spectrometer resolution. For the spectrometer settings we used here, this broadening had a minimal effect on the fit. In turn, we computed H by backfilling the vacuum chamber with rarefied nitrogen up to 1 Torr, and using the same apparatus to detect the rotational Raman scattering spectrum. We generated an analogous fitting function for the convolution of the theoretical rotational line intensities with $I(\lambda)$, following the work of Van de Sande [33]. The resulting H value accounts for the laser energy, scattering geometry, and collection optic transmission efficiency, which is identical for both scattering processes. Dashed lines in Fig. 4a and b show the stopband of the stray light filters, within which we did not consider data for the fit. The fact that the spectrum is not reduced from the neighboring values within these bounds is coincidental, suggesting that after Bragg

filtering, the intensity of the stray light from elastic (i.e. Rayleigh) and inelastic (i.e. excitation) plasma scattering as well as reflections was of comparable intensity to the Thomson spectrum.

Figure 4c shows the electron temperature and density inferred from these fits at each location. Error bars demonstrate the 95% confidence intervals obtained from least squares fitting of the model due to measurement noise. We propagated these uncertainties using the same Monte Carlo approach as was used to compute LIF properties. We see that the electron temperature scales roughly with the electric field strength (c.f. 3c), peaking < 0.1 channel lengths downstream of the thruster exit plane. This is expected, as the primary energy source for the electrons is $\vec{J} \cdot \vec{E}$ (i.e., "Ohmic") heating. However, we note here as in Ref. [23] that these large peak temperature values, ranging up to 80 eV, exceed previous probe measurements on similar devices [19, 20, 34] as well as models [16] by more than a factor of two. However, these measurements are consistent with other Thomson scattering studies of a lower-power, magnetically shielded Hall thruster [22], which also observed similarly large temperatures. This discrepancy motivates the present study, suggesting a gap in the current understanding of electron heating in the Hall thruster plume.

The electron density decreases with distance from the thruster exit plane ($z = 0$). This is consistent with the acceleration of ions (Fig. 3c), which by particle continuity must reduce the quasineutral plasma density in the downstream locations. We also note that in Figs. 4a-b, a nonzero displacement of the distributions' means from the laser wavelength is observable. This corresponds to a net drift in the azimuthal direction. While in this work we do not show these drift values, in Ref. [23] we use these drift measurements to infer the inverse Hall parameter via Ohm's law (c.f. Eq. 2).

C. Computation of Electron Heat flux

Equipped with the measurements of electric field strength from the LIF diagnostic, along with the electron properties from the ITS system, we are able to infer the divergence of the heat flux via Eq. 4. To accomplish this, we must make an assumption for the value of the total local current density, J_z, which we assume is conserved over the measurement domain. For this, we look to measurements of the global current utilization efficiency in the H9 from Ref. [35], which measured this efficiency as $\eta_B \approx 0.83 \pm 0.04$. We can therefore estimate the total current density as

$$J_z \approx \frac{e n_e u_{iz}(z_f)}{\eta_B}, \tag{11}$$

where $u_{iz}(z_f)$ is the ion velocity evaluated at the downstream end of the experimental domain (0.51 channel lengths). This assumption allows us to evaluate each term of the energy equation, the combination of which must be balanced by the final term involving the axial heat flux, θ_{ez}.

In addition to inferring the heat flux directly from the energy equation, we may use the momentum equation to extract an effective collision frequency, ν_e, which parameterizes the anomalous momentum transport of electrons. We can then use ν_e along with the classical scaling for the cross-field heat flux (Eq. 6) to evaluate the agreement of this framework with our direct inference scheme. Figure 5a displays the values of the inverse Hall parameter, $\Omega^{-1} = \nu_e/\omega_{ce}$, reproduced from Ref. [23]. In that reference, we employed an analogous approach - with the electron momentum equation instead of energy equation - to measure the collision frequency from the electron drift velocities produced in the same experiment considered herein. For comparison, we also show in Fig. 5a the classical electron-ion collision frequency in blue, noting that the effective Hall parameter is highly non-classical.

Figure 5b displays in black with 95% credible intervals our computation of the axial derivative of the heat flux, $d\theta_z/dz$, from Eq. 4. Also displayed are the relative contributions from each term in the energy equation: Ohmic heating, ionization, and convection. We see that ionization energy loss is a relatively small effect over the measured domain. In contrast, the positive value of the Ohmic heating term adds energy to the electrons in the region of ion acceleration before decreasing downstream, consistent with the measured electric field profile in Fig. 3. Finally, we see that the convection of electron pressure is the dominant contributor to the derivative of the heat flux. This is an unexpected result, and is driven by the large electron temperature gradient we observed (c.f. 4). We discuss this finding further in the following section.

For further physical insight, it is useful to evaluate the actual value of the heat flux rather than its derivative. We can only measure the derivative directly with this method, and thus the heat flux is only known up to a constant of integration. However, we note that both calculations of the derivative of the heat flux go to zero at the downstream boundary of the interrogated locations, i.e. the heat flux is constant with axial position there. Additionally, we note that classical heat flux values based on either the classical or non-classical collision rate (both curves in Fig. 5a) go to zero at the downstream boundary. We may therefore choose for the purpose of illustration a vanishing value $\theta_{ez} = 0$ at the downstream boundary of the measurement region, allowing numerical integration of the quantities in Fig. 5b. We

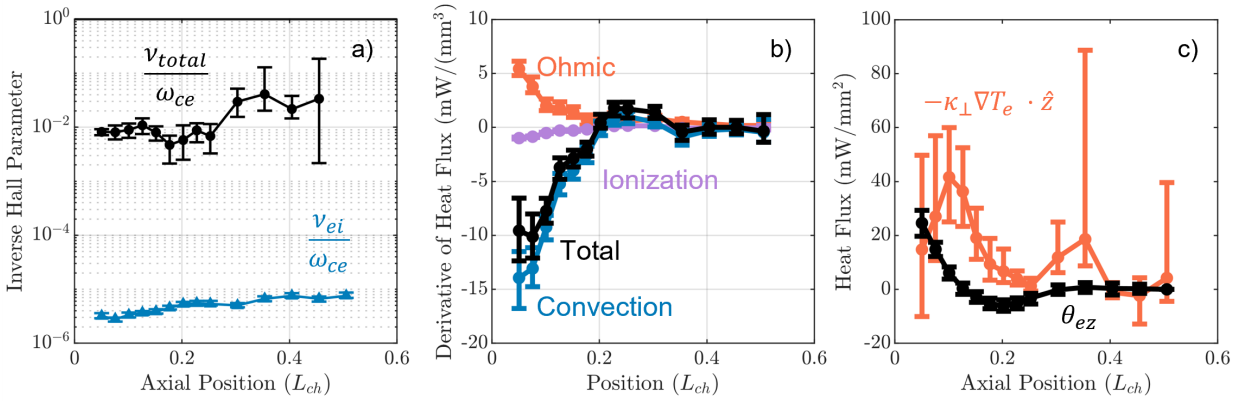

Fig. 5 a) Inverse Hall parameter, reproduced from Ref. [23] with permission. Also overlaid is the Hall parameter computed from the classical electron-ion collision rate (Eq. 7). b) Divergence of the heat flux (black) and the relative contribution from other electron heating/loss terms, including Ohmic heating (orange), ionization (purple), and convection (blue). c) Total heat flux integrated from the quantities (b), assuming a value of zero at the downstream boundary of the interrogated region for illustration. Note that the measurement of this quantity is only defined up to an additive constant. Also shown in orange is the effective collisional value of the heat flux inferred from the measured total collision rate displayed in (a).

show this estimate for the absolute cross-field heat flux value in black in Fig. 5c. Additionally, we show in orange the value of the heat flux computed from Eq. 6, using the total (anomalous) collision rate measured in Ref. [23]. We note that the cross-field heat flux due to the small, classical electron-ion collision rate would be effectively zero over the measurement domain for the shown y-axis in Fig. 5c.

Qualitatively, both estimates are positive at the exit plane of the thruster, corresponding to a downstream direction of energy conduction. Both estimates also roughly decrease with distance from the exit plane of the thruster. Quantitatively, however, the profiles are quite different. The inferred heat flux decreases below zero at the region of maximum magnetic field ($z \sim 0.2L_{ch}$), before rising again to the constant downstream value (assumed zero). Meanwhile, the value of the collisional heat flux remains large for a more significant portion of the acceleration region, before eventually falling to smaller values downstream of 0.16 channel lengths from the exit plane. In some locations in the acceleration region, these estimates disagree in sign and by a value of $\sim$ 40 mW/mm^2. We note that while some modeling work does predict a sign change in the heat flux (c.f. Ref. [11]), this sign change may also be an artifact of our choice to set the constant of integration such that the downstream heat flux to zero; if this approximately constant downstream value is in reality nonzero, the heat flux vector could point downstream throughout the entire acceleration region. Despite this, the disagreement between the measured and collisional heat flux profiles makes clear that the collisional estimate for the heat flux is not necessarily an appropriate approximation for the actual value within the Hall thruster plume. In the following, we discuss further implications and limitation of these findings.

V. Discussion

In this section, we discuss the implications of the results from Sec. IV in the context of previous studies, as well as comment on the limitations of the methodology employed here.

A. Implications for Plasma Models

The work presented herein demonstrates that the cross-field electron heat flux, as inferred from non-intrusive, laser scattering measurements of the ion and electron properties in a laboratory Hall thruster, does not agree with a classical formulation based on the momentum transfer collision frequency. While the collisional prediction of the electron heat flux displays qualitatively similar behavior, namely energy transport in the downstream direction which peaks at the acceleration region and decays with axial distance, the actual region of this elevated heat flux is displaced upstream axially by a significant amount relative to the collisional prediction, as shown in Fig. 5c. This discrepancy arises mathematically because the measured electron temperature has a local maximum at the exit plane (Fig. 4c), while the

inverse Hall parameter is nearly constant there (Fig. 5a). A description of the heat flux based on Fourier's law (Eq. 5) with classical temperature scaling therefore predicts little change in the heat flux with distance, due to the very small electron temperature gradient at the maximum. In contrast, the heat flux value inferred from the energy scales differently with electron pressure, including the effects of axial drift velocity. Indeed, the bulk cross-field electron migration toward the anode convects significant thermal energy upstream from this region of high temperatures, requiring the electrons to conduct a similar amount of energy in the downstream direction to balance the transport. The change in internal heat flux that results from this energy balance is therefore more negative at the exit plane, resulting in a heat flux value that decays much more quickly than the collisional estimate.

This finding represents a large departure from previous investigations of similar Hall thrusters, which generally employ collision-frequency-based methods for estimating the heat flux [4, 12, 13, 15]. A growing body of evidence supports the conclusion that the bulk of anomalous electron migration across field lines is driven by interactions with plasma turbulence, and in particular is related to the electron cyclotron drift instability (ECDI) [8, 36, 37]. The nonlinear interactions with plasma waves which may cause anomalous momentum and energy transport likely contribute to the energy equation in complex ways, which depend on the dispersion relation and growth rates of the relevant instabilities [36, 38]. For this reason, it is likely that including these kinetic plasma effects in models of the electron transport as a Fourier-like thermal conductivity parameter would require adopting a correspondingly complex temperature dependence in said parameter, rather than assuming that the wave interactions randomize the electron velocity in the same manner as collisions with classical particles. We note the striking result that the electron heat conduction across field lines is predominantly a result of the need to balance strong convection in this region of the discharge, and that Ohmic heating is only a small effect in this regard. Based on this finding, it is possible that closure models for the electron fluid energy equation may find a more appropriate prescription by accounting for the anomalous heat flux with a convective-like energy term, for example $\theta_{ez} \sim -5/2 p_e u_{ez} + C$, where C is a constant of integration.

B. Methodological Limitations

While these results are relatively robust, we here acknowledge limitations with the methodology employed. The chief limitation is the assumption that our measurements of the azimuthal electron temperature are representative of the axial electron temperature, which is the quantity which is directly related to the cross-field transport. While both directions are perpendicular to the magnetic field, the strong azimuthal drift and axial electric field could lead to three-dimensional anisotropy in the electron temperature, which could potentially imply different conclusions. The same assumption was used in Ref. [23] to infer the inverse Hall parameter, and this conclusion is subject to the same caveat. However, we note here the good agreement of the measured Thomson spectra with Maxwellian fits. This suggest that at least in the azimuthal direction, there is sufficient velocity randomization, collisional or otherwise, to drive the electron population toward an equilibrium state. Also, in Ref. [23], we show that predictions of the azimuthal electron drift which compute the diamagnetic contribution from the azimuthal temperature agree well with our direct measurements of this velocity, further validating this assumption.

A secondary limitation is the simplified electron energy equation we adopt in this work. In particular, we neglect energy transfer from the electron to other species such as ions and neutrals, as well as any 2D effects such as azimuthal/radial asymmetries. However, such effects are likely small on channel centerline given the plasma conditions [4, 20]. If significant radial gradients do exist along the field lines, both our formulation and most models would require reassessment - we note that this would also imply reduced thermal transport in the radial direction, which could likewise contribute to the large observed electron temperatures. We note additionally that this study was performed on a magnetically shielded thruster, which exhibits a highly curved magnetic field. The magnetic field lines in the acceleration region thus terminate at the front magnetic pole rather than intersecting the channel walls, pushing the acceleration region downstream [19, 34, 39]. While this is a state-of-the-art, flight-like Hall thruster configuration, these results may not be representative of traditional, unshielded Hall thrusters with different discharge properties. Finally, these results depend on a free parameter J_z, the axial current density, which we estimate with uncertainty from the measured ion current density and global performance measurements; we assume J_z is constant throughout the measurement region. This ignores any plume divergence, which could reduce the value of J_z locally due to the expanding effective area which the beam current flows through as it diverges. However, the results are relatively insensitive to the small changes in this value which would result from realistic expansion values. Our neglect of both beam divergence as well as the off-axis, radial heat transport and pressure balance motivate future studies examining the 2D heat flow in magnetically shielded Hall thrusters. Despite these concessions, however, the results of these non-intrusive measurements make clear the gap between existing implementations of energy equation closure in Hall thruster models and actual local thruster dynamics.

VI. Conclusion

In summary, in this work we have demonstrated a diagnostic approach to directly measure the electron heat flux in a crossed-field plasma. We developed a formulation for this quantity based on the conservation of energy in a Hall thruster acceleration region, accounting for heating of the electrons by the electric field work, energy loss to ionization collisions, and convection of pressure in the direction perpendicular to the magnetic field. By combining this mathematical approach with azimuthal measurements of the electron temperature and density taken with a Thomson scattering diagnostic, as well as measurements of the ion velocity from a laser-induced fluorescence diagnostic, we were able to resolve the axial gradient of the electron heat flux throughout the near-field plume of a magnetically shielded Hall thruster operating at 4.5-kW on krypton propellant. This result allowed for straightforward evaluation of the application of the classical, Braginskii closure for cross-field heat flux to anomalous electron transport in this low-temperature, cross-field plasma source.

We found that the value of the electron heat flux predicted by the energy equation differs significantly compared to the collision-based prediction. In particular, we found that positive values of the heat flux quickly drop off with distance from the exit plane, to the point that the axial heat flux may change direction. This trend is driven by the large localized peak in electron temperature (up to a value of ~ 80 eV), which induces a large pressure gradient that in turn causes significant downstream heat flux. In contrast, the heat flux predicted from the experimentally measured anomalous collision frequency remains large throughout the region of peak electric field in the thruster, before eventually falling to agreement near 0.5 channel lengths from the thruster. The disagreement between these quantities in the acceleration region is a significant finding, as existing Hall thruster models generally treat energy transport collisionally. This result suggests a path forward for modeling and experiment which involves relaxing typical assumptions about the magnitude of the electron temperature, and the nature of electron diffusion and heating in Hall thrusters.

Acknowledgments

This work was supported by a NASA Space Technology Graduate Reseach Opportunity (Grant 80NSSC20K1229). In addition, the authors would like to thank Dr. Zachariah Brown, Madison Allen, and William Hurley for experimental assistance, in addition to Dr. Leanne Su for providing modeling results.

References

[1] Goebel, D. M., Katz, I., and Mikellides, I. G., *Fundamentals of electric propulsion*, John Wiley & Sons, 2023.

[2] Boeuf, J.-P., "Tutorial: Physics and modeling of Hall thrusters," *Journal of Applied Physics*, Vol. 121, No. 1, 2017.

[3] Hofer, R. R., and Gallimore, A. D., "High-specific impulse Hall thrusters, part 2: efficiency analysis," *Journal of Propulsion and Power*, Vol. 22, No. 4, 2006, pp. 732–740.

[4] Mikellides, I. G., and Katz, I., "Numerical simulations of Hall-effect plasma accelerators on a magnetic-field-aligned mesh," *Physical Review E*, Vol. 86, No. 4, 2012, p. 046703.

[5] Bellan, P. M., *Fundamentals of plasma physics*, Cambridge university press, 2008.

[6] Meezan, N. B., Hargus Jr, W. A., and Cappelli, M. A., "Anomalous electron mobility in a coaxial Hall discharge plasma," *Physical Review E*, Vol. 63, No. 2, 2001, p. 026410.

[7] Dale, E. T., and Jorns, B. A., "Non-invasive time-resolved measurements of anomalous collision frequency in a Hall thruster," *Physics of Plasmas*, Vol. 26, No. 1, 2019.

[8] Brown, Z. A., and Jorns, B. A., "Anomalous cross-field transport in a Hall thruster inferred from direct measurement of instability growth rates," *Physical Review E*, Vol. 108, No. 6, 2023, p. 065204.

[9] Morozov, A., and Savelyev, V., "Fundamentals of stationary plasma thruster theory," *Reviews of plasma physics*, 2000, pp. 203–391.

[10] Mikellides, I. G., Jorns, B., Katz, I., and Lopez Ortega, A., "Hall2De simulations with a first-principles electron transport model based on the electron cyclotron drift instability," *52nd AIAA/SAE/ASEE Joint Propulsion Conference*, 2016, p. 4618.

[11] Ahedo, E., Gallardo, J., and Martınez-Sánchez, M., "Model of the plasma discharge in a Hall thruster with heat conduction," *Physics of Plasmas*, Vol. 9, No. 9, 2002, pp. 4061–4070.

[12] Fife, J. M., "Hybrid-PIC modeling and electrostatic probe survey of Hall thrusters," Ph.D. thesis, Massachusetts Institute of Technology, 1998.

[13] Marks, T. A., and Jorns, B. A., "Evaluation of algebraic models of anomalous transport in a multi-fluid Hall thruster code," *Journal of Applied Physics*, Vol. 134, No. 15, 2023.

[14] Parra, F., Ahedo, E., Fife, J., and Martinez-Sanchez, M., "A two-dimensional hybrid model of the Hall thruster discharge," *Journal of Applied Physics*, Vol. 100, No. 2, 2006.

[15] Marks, T. A., and Jorns, B. A., "Challenges with the self-consistent implementation of closure models for anomalous electron transport in fluid simulations of Hall thrusters," *Plasma Sources Science and Technology*, Vol. 32, No. 4, 2023, p. 045016.

[16] Su, L. L., Marks, T. A., and Jorns, B. A., "Investigation into the Efficiency Gap between Krypton and Xenon Operation on a Magnetically Shielded Hall Thruster," *Proceedings of the 37th International Electric Propulsion Conference*, Electric Rocket Propulsion Society, Boston, MA, 2022.

[17] Lopez Ortega, A., Mikellides, I. G., Sekerak, M. J., and Jorns, B. A., "Plasma simulations in 2-D (rz) geometry for the assessment of pole erosion in a magnetically shielded Hall thruster," *Journal of Applied Physics*, Vol. 125, No. 3, 2019.

[18] Linnell, J. A., and Gallimore, A. D., "Internal plasma potential measurements of a Hall thruster using xenon and krypton propellant," *Physics of plasmas*, Vol. 13, No. 9, 2006.

[19] Mikellides, I. G., Katz, I., Hofer, R. R., and Goebel, D. M., "Magnetic shielding of a laboratory Hall thruster. I. Theory and validation," *Journal of Applied Physics*, Vol. 115, No. 4, 2014.

[20] Jorns, B., Goebel, D. M., and Hofer, R. R., "Plasma perturbations in high-speed probing of Hall thruster discharge chambers: Quantification and mitigation," *51st AIAA/SAE/ASEE Joint Propulsion Conference*, 2015, p. 4006.

[21] Grimaud, L., Pétin, A., Vaudolon, J., and Mazouffre, S., "Perturbations induced by electrostatic probe in the discharge of Hall thrusters," *Review of Scientific Instruments*, Vol. 87, No. 4, 2016.

[22] Vincent, B., Tsikata, S., and Mazouffre, S., "Incoherent Thomson scattering measurements of electron properties in a conventional and magnetically-shielded Hall thruster," *Plasma Sources Science and Technology*, Vol. 29, No. 3, 2020, p. 035015.

[23] Roberts, P. J., and Jorns, B. A., "Laser Measurement of Anomalous Electron Diffusion in a Crossed-Field Plasma (Manuscript Submitted for Review)," 2023, pp. arxiv–2312.10552.

[24] Braginskii, S., "Transport processes in a plasma," *Reviews of plasma physics*, Vol. 1, 1965, p. 205.

[25] Fitzpatrick, R., "Introduction to plasma physics," , 2004.

[26] Hofer, R. R., Cusson, S. E., Lobbia, R. B., and Gallimore, A. D., "The H9 magnetically shielded Hall thruster," *35th International Electric Propulsion Conference*, Electric Rocket Propulsion Soc., 2017, pp. 2017–232.

[27] Viges, E. A., Jorns, B. A., Gallimore, A. D., and Sheehan, J., "University of Michigan's upgraded large vacuum test facility," *36th International Electric Propulsion Conference*, 2019, pp. 1–18.

[28] Dankanich, J. W., Walker, M., Swiatek, M. W., and Yim, J. T., "Recommended practice for pressure measurement and calculation of effective pumping speed in electric propulsion testing," *Journal of Propulsion and Power*, Vol. 33, No. 3, 2017, pp. 668–680.

[29] Roberts, P. J., and Jorns, B., "Characterization of Electron Mach Number in a Hollow Cathode with Thomson Scattering," *AIAA SCITECH 2023 Forum*, 2023, p. 0843.

[30] Vincent, B., Tsikata, S., Mazouffre, S., Minea, T., and Fils, J., "A compact new incoherent Thomson scattering diagnostic for low-temperature plasma studies," *Plasma Sources Science and Technology*, Vol. 27, No. 5, 2018, p. 055002.

[31] Pérez-Luna, J., Hagelaar, G., Garrigues, L., and Boeuf, J.-P., "Method to obtain the electric field and the ionization frequency from laser induced fluorescence measurements," *Plasma Sources Science and Technology*, Vol. 18, No. 3, 2009, p. 034008.

[32] Sheffield, J., Froula, D., Glenzer, S. H., and Luhmann Jr, N. C., *Plasma scattering of electromagnetic radiation: theory and measurement techniques*, Academic press, 2010.

[33] Van de Sande, M., "Laser scattering on low temperature plasmas," *Eindhoven University of Technology, Eindhoven*, 2002.

[34] Hofer, R. R., Goebel, D. M., Mikellides, I. G., and Katz, I., "Magnetic shielding of a laboratory Hall thruster. II. Experiments," *Journal of Applied Physics*, Vol. 115, No. 4, 2014.

[35] Su, L., and Jorns, B., "Performance comparison of a 9-kW magnetically shielded Hall thruster operating on xenon and krypton," *Journal of Applied Physics*, Vol. 130, No. 16, 2021.

[36] Hara, K., and Tsikata, S., "Cross-field electron diffusion due to the coupling of drift-driven microinstabilities," *Physical Review E*, Vol. 102, No. 2, 2020, p. 023202.

[37] Brown, Z. A., and Jorns, B. A., "Growth and Saturation of the Electron Drift Instability in a Crossed Field Plasma," *Physical Review Letters*, Vol. 130, No. 11, 2023, p. 115101.

[38] Davidson, R., and Krall, N., "Anomalous transport in high-temperature plasmas with applications to solenoidal fusion systems," *Nuclear Fusion*, Vol. 17, No. 6, 1977, p. 1313.

[39] Cusson, S. E., Dale, E. T., Jorns, B. A., and Gallimore, A. D., "Acceleration region dynamics in a magnetically shielded Hall thruster," *Physics of Plasmas*, Vol. 26, No. 2, 2019.